

Cluster-Group Interaction in the Virgo Cluster

S. Schindler

University of Innsbruck, Institute for Astrophysics, Technikerstr. 25, 6020 Innsbruck, Austria

We present two projects related to interaction in the Virgo cluster. In the first section we draw a quantitative comparison of the distribution of the galaxies and the intra-cluster gas taking into account that the Virgo cluster has an irregular structure consisting of several subclusters. In the second section we show hydrodynamic simulations of the interaction (ram pressure stripping) of a galaxy like M86 with the intra-cluster gas.

1 Comparison of the optical and the X-ray morphology of the Virgo cluster

The Virgo cluster, as the nearest cluster of galaxies, is ideally suited for a detailed comparison of the distribution of two components – intra-cluster gas and galaxies.

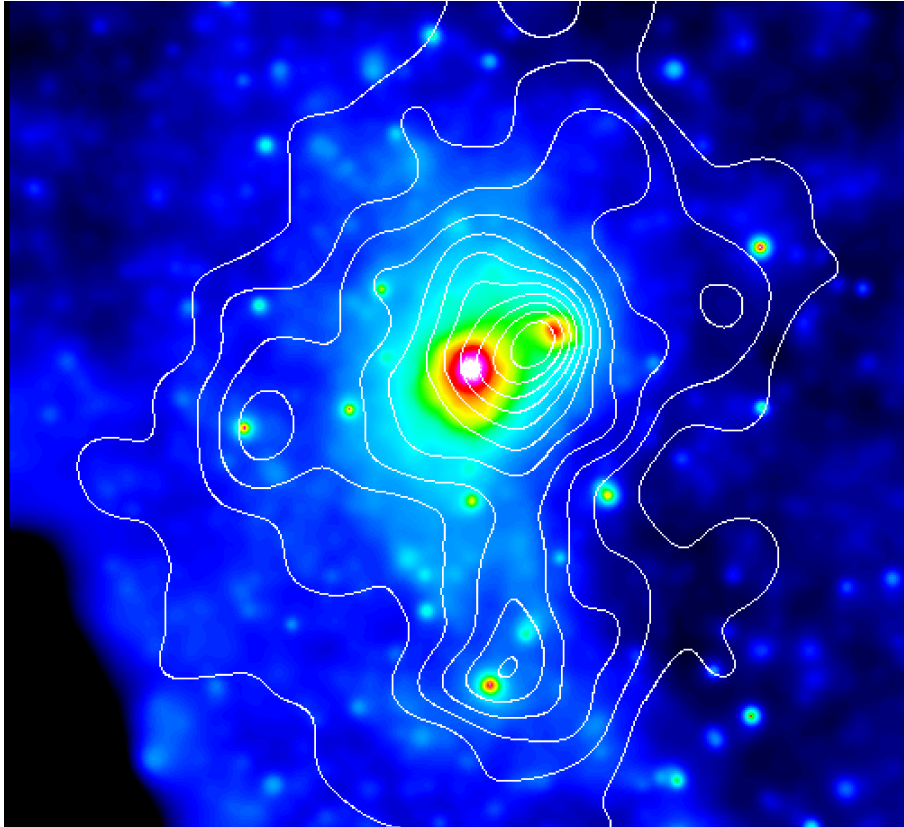


Figure 1: Comparison of the X-ray and the optical appearance of the Virgo cluster. The colour image shows the X-ray emission as observed by the ROSAT All-Sky Survey in the hard band (0.5-2.0 keV). It is smoothed with a Gaussian filter with $\sigma = 24$ arcmin on the faintest levels and decreasing filter size with increasing surface brightness. The contours show the number density of the 1292 member galaxies of the VCC smoothed again with a Gaussian of $\sigma = 24$ arcmin. The spacing of the contours is linear. The lowest contour line and the contour spacing is 1.5×10^{-3} galaxies per arcmin². The image has a size of $12.8^\circ \times 12.8^\circ$. North is up and West to the right. The main X-ray maximum is centred on M87 ($\alpha_{2000} \approx 12^{\text{h}}30^{\text{m}}$, $\delta_{2000} \approx 12^{\text{circ}}23$ arcmin). For the identification of further galaxies, cf. Fig. 2.

Figures 1 and 2 show the distribution of both components. The Virgo cluster is obviously a complex system. There is a pronounced double structure in the direction N-S. The Northern clump, called “cluster A” in (Binggeli et al. 1987, BTS87), is dominated by M87, which coincides with the maximum of the X-ray emission in the whole area. The Southern, much less pronounced clump, coincides with M49, another supergiant elliptical that is even slightly brighter than M87. However, as emphasized in BTS87, the galaxy density contours do not peak on M87 but almost 1° WNW of it – more than halfway in the direction to M86, which is yet another giant E galaxy (see Fig. 2a). The reason for this “mispointing” of M87 is now clear: the Northern clump itself is a double system comprising the dominating, massive subcluster centred on M87 and a smaller subcluster centred on M86. This view is supported by the existence of a swarm of low-velocity dwarf galaxies around M86 (which itself has a negative velocity, Binggeli et al. 1993) and the extended X-ray halo of M86 (Forman et al. 2001). The M86 subcluster seems to fall into the M87 subcluster from behind.

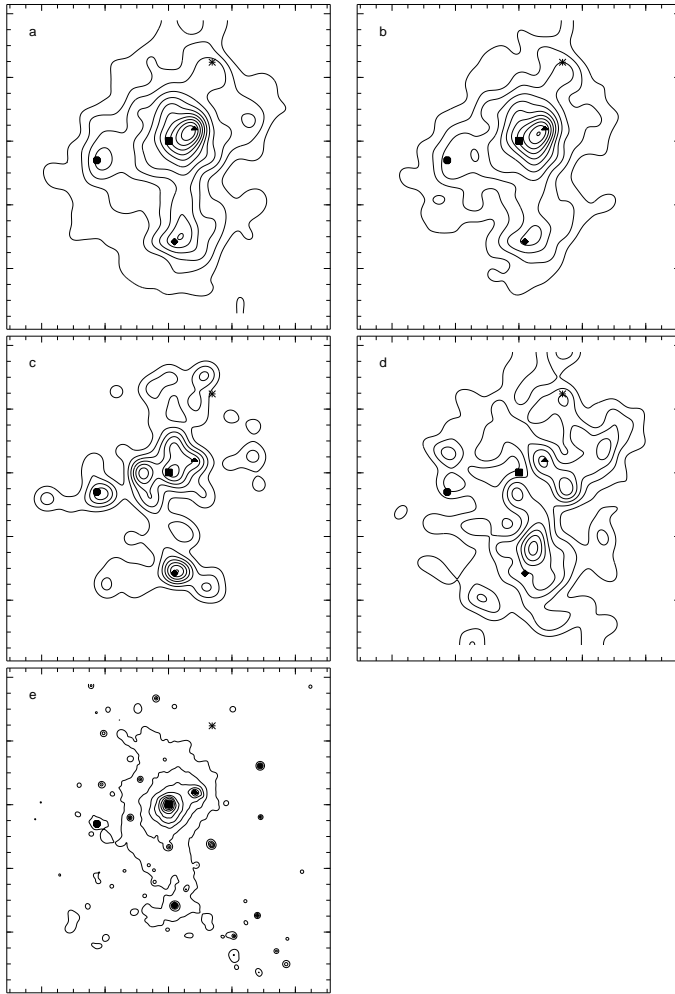


Figure 2: Distributions of the different galaxy types. Number densities smoothed with a Gaussian of $\sigma = 24$ arcmin are shown. (a) all galaxy types, (b) dwarf elliptical and dwarf S0 galaxies, (c) elliptical and S0 galaxies, (d) spiral and irregular galaxies. The contours are linear with spacings of (a) 1.5×10^{-3} galaxies/arcmin², (b) 1.3×10^{-3} galaxies/arcmin², (c) 2.2×10^{-4} galaxies/arcmin², (d) 3.6×10^{-4} galaxies/arcmin². The level of the first contour line is equal to the spacing. For better comparison with Fig. 1 the positions of five galaxies are marked: M87 (square), M49 (diamond), M86 (triangle), M60 (octagon), M100 (star). (a) is the same as the contours in Fig. 1. For comparison the X-ray image is shown again in (e) with logarithmically spaced contours. The size of each image is $12.8^\circ \times 12.8^\circ$. The distance between two tick marks is 42 arcmin.

Table 1: Masses of the subclusters centred on M87, M49 and M86 (integrated values). Galaxy masses are based on a constant $\mathcal{M}_\odot/\mathcal{L}_{\odot,B}$ of 20. The total masses of the subclusters were calculated on the assumption of an isothermal gas. The 1σ error for the galaxy masses is $\approx 20\%$, that for the total masses is 30-50% (except for M86).

	M87		M49		M86
	($r=400\text{kpc}$)	($r=1\text{Mpc}$)	($r=400\text{kpc}$)	($r=750\text{kpc}$)	($r=240\text{kpc}$)
$M_{tot}[10^{13}\mathcal{M}_\odot]$	5.5	14	4.7	8.7	1 – 3
$M_{gas}[10^{13}\mathcal{M}_\odot]$	0.42	1.9	0.026	0.044	-
$M_{gal}[10^{13}\mathcal{M}_\odot]$	0.14	0.51	0.17	0.34	0.06
M_{gas}/M_{tot}	8%	14%	0.6%	0.5%	-
M_{gal}/M_{tot}	3%	4%	4%	4%	2 – 6%
M_{gal}/M_{gas}	0.34	0.28	6.6	7.7	-
$M/L[\mathcal{M}_\odot/\mathcal{L}_{\odot,B}]$	≈ 500	≈ 500	≈ 500	≈ 600	300 – 1000

We thus deal essentially with three major subclusters centred on the giant ellipticals M87, M86, and M49. They are readily visible as maxima in Fig. 1. Note that these X-ray sources are not point sources but are extended: the hot gas is located in the potential of the (extended) subclusters.

The number density distribution for the various galaxy types in the Virgo cluster is shown in Fig. 2b (early-type dwarfs, i.e. dE and dS0), 2c (early-type giants, i.e. E and S0), and 2d (late types, i.e. spirals and irregulars). Confirming the results of BTS87 we find very different distributions for the different types. The dwarf ellipticals (Fig. 2b) have a distribution very similar to that of all galaxies (Fig. 2a), simply because they make up 3/4 of the total cluster population. The ellipticals and S0s (Fig. 2c) show a less extended distribution and are more concentrated to the subcluster centres, i.e. the X-ray maxima (compare with Fig. 2e). In sharp contrast, the distribution of the spirals and irregulars (Fig. 2d) is very extended and shows no correlation with the X-ray emission. Note also the difference in the type-mix between the various clumps. The M49 subcluster is obviously spiral-rich.

For both components – gas and galaxies – we have fitted the observed subcluster profiles with isothermal β -models, which allow an easy deprojection to three-dimensional densities. The comparison of the X-ray and optical density profiles of the Virgo subclusters has led to the following results:

- The X-ray profile is steeper than the optical profile in the central part ($r < 70$ arcmin) but with a slight inverse trend at larger radii – for both the M87 and M49 subclusters. This is reflected in the much smaller X-ray core radii and the smaller X-ray β -values than the corresponding optical values.
- The more massive the subcluster the less compact is its structure - both in optical and in X-rays, i.e. poorer subclusters have a steeper radial profile. This behaviour is in agreement with the results of N-body simulations by Navarro et al. (1997) who also found steeper profiles for low-mass haloes than for high-mass haloes. The same systematic effect is well-known to hold also for normal elliptical galaxies, i.e. low-luminosity ellipticals (like M32, but unlike “dwarf” ellipticals) appear much more compact than giant ellipticals.
- Different Hubble types show different slopes in the subcluster profiles. We confirm the results by BTS87 that early-type galaxies are much more strongly clustered than late-type galaxies, reflecting of course the well-known morphology-density relation (Dressler 1980).
- There is a region South-West of M87 which shows a steeper gradient than the rest of the M87 subcluster - both in the optical and in X-rays. Such steep gradients in the X-ray emission can be caused by shock waves emerging after the collision and merging of subclusters (Schindler & Müller 1993).
- Differential and integrated profiles of the galaxy mass, gas mass, and total gravitating mass density are studied for both the M87 subcluster and the M49 subcluster (see Table 1). The gas

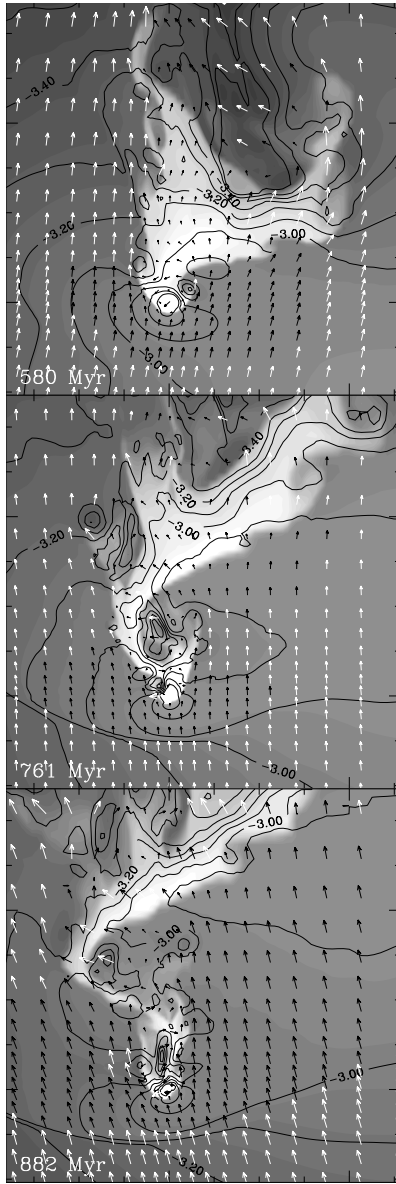


Figure 3: Gas density (grey scale) and pressure (contours) of a galaxy moving downwards towards the cluster centre. The arrows show the Mach vectors (white when $M > 1$, black otherwise). The gas of the galaxy is stripped due to ram pressure.

mass fraction in M87, with 8% and 14% at 400 kpc and 1 Mpc, respectively, is slightly on the low side for clusters, but is still in the normal range. One finds the usual behaviour that the gas distribution is somewhat flatter than the distribution of the total mass, i.e. the gas distribution is more extended. The integrated gas mass is about 3 times the galaxy mass. This is about the same factor that was found in other clusters. A comparison of the gravitating mass of the M87 subcluster ($M_{tot,M87} = 2.1 \times 10^{14} \mathcal{M}_{\odot}$) with the masses of other clusters shows that they are in general more massive than the M87 subcluster, e.g. the Coma and the Perseus cluster have almost a factor of ten more gravitating mass. The galaxy mass density is getting flatter towards the centre, which is the reason why the mass-to-light ratio also tends to increase with decreasing radius (excluding M87 itself, i.e. for $r < 60$ arcmin). We find projected mass-to-light ratios between 300 and 500 $\mathcal{M}_{\odot}/\mathcal{L}_{\odot,B}$ at radii larger than 200 kpc which are relatively large mass-to-light ratios compared to the values of 90-250 $h_{50} \mathcal{M}_{\odot}/\mathcal{L}_{\odot}$ generally found in other clusters.

The mass distributions for the M49 subcluster are similar. The only quantity which differs substantially between the M87 and M49 subclusters, however, is the gas mass fraction. For the

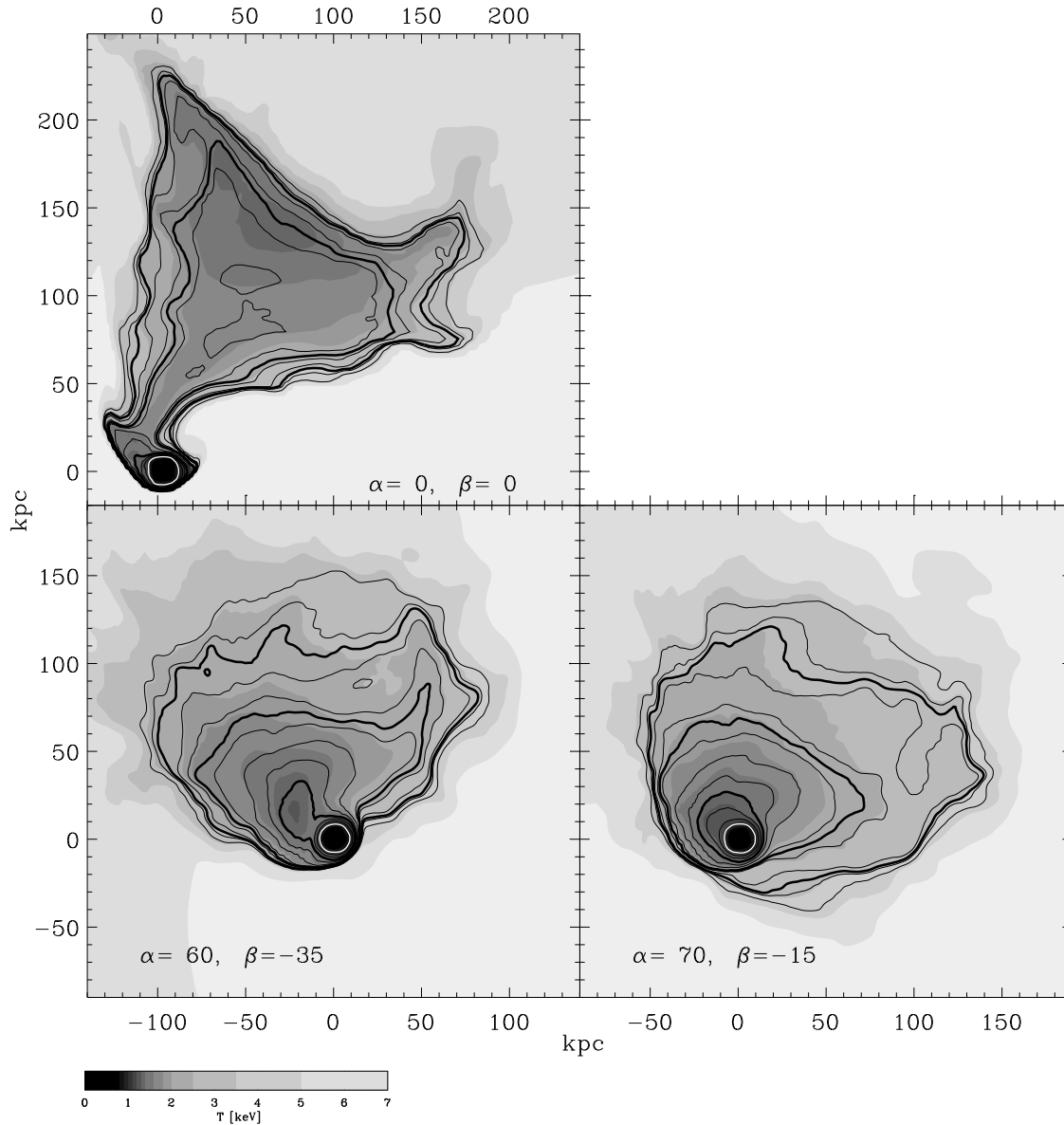


Figure 4: Simulated X-ray images (contours) and temperatures (grey scale) of a galaxy affected by ram-pressure stripping in three different projection directions.

M49 subcluster we find a very small gas mass fraction of less than 1% of the total mass. For more details on the comparison between the gas and the galaxy distribution see Schindler et al. (1999).

2 Ram-pressure stripping of M86-like galaxies

We performed hydrodynamic simulations of ram-pressure stripping of elliptical galaxies as they pass through the intra-cluster gas. We considered different orbits of the galaxies through the cluster.

An example of such a stripping process is shown in Fig. 3. We find Kelvin-Helmholtz wiggles developing on the ISM-ICM interface, which produce secondary shocks and secondary rarefaction fans on the sides downstream of the galaxy centre. Irregular extensions of the ISM form, which grow or stretch until they break away. Initially, the momentum acquired by the ISM is spent in climbing up the galaxy’s potential well, so that for some time the ISM is almost co-moving with the galaxy. As soon as the ISM is displaced and decelerated, it starts falling towards the cluster

centre. A second shock is formed in front of the stripped, flowing material. The pressure built up behind the second shock in turn displaces the ISM upstream. This produces the “S”-shape of the trail visible in Fig. 3.

We find that the gas cannot only be stripped off as the galaxy approaches the cluster centre, but the galaxy can again accumulate some gas when it is in the apocentre of its orbit.

Also the X-ray morphologies of the stripped galaxies and their X-ray temperature maps can be calculated (Fig. 4) for direct comparison with observations, like e.g. the X-ray morphology and temperature map of M86 as observed by CHANDRA (Forman et al. 2001)

For more details on the hydrodynamic simulations of the ram-pressure stripping process see Toniazzo & Schindler (2001).

References

- Binggeli B., Tammann G.A., Sandage A., 1987, AJ 94, 251 (= BTS87)
Binggeli B., Popescu C.C., Tammann G.A., 1993, A&AS 98, 275
Dressler A., 1980, ApJ 236, 351
Forman W., et al., 2001, *Proceedings of the XXI Moriond Conference: Galaxy Clusters and the High Redshift Universe Observed in X-rays*, Neumann D.M. (ed.)
Navarro J.F., Frenk C.S., White S.D.M., 1997, ApJ 490, 493
Schindler S., Binggeli B., Böhringer H., 1999, A&A 343, 420
Schindler S., Müller E., 1993, A&A 272, 137
Toniazzo T., Schindler S., 2001, MNRAS 325, 509